Journal of Alloys and Compounds 505 (2010) 661–667

Contents lists available at ScienceDirect

Journal of Alloys and Compounds

journal homepage: www.elsevier.com/locate/jallcom

Compositional effect on structural and spectroscopic properties of P_2O_5–SnO–MnO ternary glass system

Woon Jin Chung [a,*], Jeon Choi [a], Yong Gyu Choi [b]

[a] Institute for Rare Metals & Division of Advanced Materials Engineering, Kongju National University, Cheonan, Chungnam, 330-717, Republic of Korea
[b] Department of Materials Science and Engineering, Korea Aerospace University, Goyang, Gyeonggi, 412-791, Republic of Korea

ARTICLE INFO

Article history:
Received 4 May 2010
Received in revised form 14 June 2010
Accepted 16 June 2010
Available online 25 June 2010

Keywords:
Inorganic
Amorphous and optical materials
Luminescence
Optical properties
Optical spectroscopy

ABSTRACT

Glasses with a P_2O_5–SnO–MnO ternary system were synthesized and characterized. Glass forming range was determined to be 5–20 mol% of MnO when the content of SnO was kept below 50 mol%. Various analyses including thermal, optical and structural characterization were performed on $(85-x)P_2O_5$–xSnO–15MnO (x = 30, 35, 40 and 45 in mol%) and $(55-y)P_2O_5$–45SnO–yMnO (y = 0, 5, 10 and 15 in mol%) glasses in order to investigate the compositional effect of SnO and MnO on the properties of glass. Glass transition temperature of all the prepared glass samples turned out to be below 350 °C, but showed a compositional dependency on SnO and MnO, which was discussed in terms of the structural changes derived from Raman spectroscopy. The visible transparency of both glass series was identified with their high optical bandgap of 3.4–3.7 eV and their refractive indices varied between 1.6 and 1.9 depending on the wavelength monitored and composition. Er^{3+} doped the glasses to examine their potential as a photonic gain medium. Radiative emission properties, Judd–Ofelt analysis and stimulated emission cross-sections also exhibited the influence of SnO and MnO and suggested the preferred concentrations of SnO and MnO as 35 mol% and 5 mol%, respectively. Modification of the local structure around the Er^{3+}-ion upon the compositional variation was responsible for the phenomena. This is also discussed with the structural contribution of SnO and MnO.

1. Introduction

Phosphate glasses have unique properties such as low softening temperatures and excellent transparency at UV and visible wavelengths, and thus have been actively studied for practical applications [1–5]. For example, their low softening temperature allows them to be used to develop Pb-free sealing materials based on phosphate glasses [6,7]. Some phosphate glasses containing BaO, CaO, SnO or ZnO have been proposed as replacements for the Pb-rich glasses that show a low glass transition temperature and a high thermal expansion coefficient [8–11]. On the other hand, phosphate glasses incorporating transition metal oxides are known to be semiconducting, which promises potential applications as electrical materials [12–14]. The small polaron hopping occurring between multi-valenced transition metal ions was reported to be responsible for electronic conduction, but the measured conductivities were low in most phosphate glasses [12–14]. However, phosphate glass containing SnO was applied to the anode material of a Li-secondary battery [9,15].

As for optoelectronic applications of phosphate glasses, these are considered promising due to their high solubility and stimulated emission cross-section of rare-earth ions [1,16–20]. Er^{3+}-doped phosphate optical fiber [21] and waveguides [18] have already been demonstrated, thus proving their potential as photonic materials. Recently, modification of phosphate glass structures has been tried not only to improve the chemical stability of phosphate glass but also to enhance the quantum efficiency of rare-earth dopants; some instances include the formation of nanocrystals of rare-earth phosphate [16] and the introduction of fluoride or chloride phases into a phosphate host matrix [19,20].

Based on the above considerations, it is inferred that a proper host matrix based on phosphate glass can be adapted to various applications exploiting its thermal, electronic or photonic characteristics. Among the various transition metal oxides that can be accommodated well with P_2O_5, a MnO–P_2O_5 system forms a stable amorphous state, and is also known to have further increased electrical conductivity [12]. It is also known that the binary phosphate system, i.e., SnO–P_2O_5, exhibits good electrical conductivity [8]. We notice that a ternary phosphate system in SnO–MnO–P_2O_5 compositions may feature some interesting electrical and optical

* Corresponding author at: Division of Advanced Materials Engineering, Kongju National University, 275 Budae-dong, Seobuk-gu, Cheonan, Chungnam, 330-717, Republic of Korea. Tel.: +82 41 521 9377; fax: +82 41 568 5776.
E-mail address: wjin@kongju.ac.kr (W.J. Chung).

0925-8388/$ – see front matter © 2010 Elsevier B.V. All rights reserved.
doi:10.1016/j.jallcom.2010.06.104

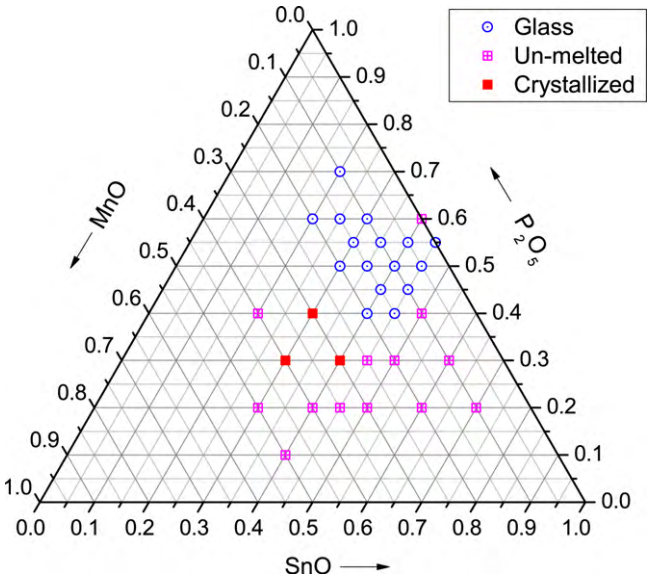

Fig. 1. Glass forming range of P_2O_5–SnO–MnO ternary system.

characteristics. However, there has been no previously reported work carried out upon the synthesis and spectroscopic characterization of this ternary system. As such, in this study, we have aimed at verifying its glass forming region and characterizing its thermal, structural and optical properties. In addition, its applicability as a host matrix of rare-earth ions was examined with glass samples doped with Er, which was chosen as a representative rare-earth element in this study. The compositional effects of SnO and MnO on these properties were then discussed.

2. Experimental

Starting materials of P_2O_5, SnO and MnO, all of high purity better than 99.99% (Kojundo Chemical Lab Co., Japan), were batched in the following compositional ranges: 10–70 mol% of P_2O_5, 20–70 mol% of SnO and 0–50 mol% of MnO. According to the batched compositions, melting temperatures were varied between 1100 °C and 1400 °C at which every batch was maintained for 30 min in an alumina crucible under ambient atmosphere. Quenching was carried out by pouring the melts on a brass mold. Thus the resulting samples were then annealed at 300 °C for 6 h to relax the thermal stresses involved. All samples were cut into a disk shape with a thickness of around 1 mm and optically polished for the following measurements. Among the compositions inside the glass forming region, glasses of $(85-x)P_2O_5$–(x)SnO–15MnO with x = 30, 35, 40 or 45 in mol% (designated PS glasses hereafter) and $(55-y)P_2O_5$–45SnO–(y)MnO with y = 0, 5, 10 or 15 (PM glasses) were selected in order to investigate the compositional effects of SnO and MnO. In addition, Er_2O_3 of 1 mol% was doped into both PM and PS glasses to examine the spectroscopic properties of Er^{3+} ions. All glass samples were prepared in an ambient atmosphere.

The temperatures of glass transition (T_g) and crystallization (T_x) were measured using a differential scanning calorimeter (DSC-60, Shimadzu Corporation). A UV/VIS/NIR spectrophotometer (PerkinElmer Lambda 750, PerkinElmer) was used to record absorption spectra. Structural changes upon the compositional variation were monitored with a Raman spectrometer (SPEX1403, HORIBA Jobin-Yvon Ltd.) equipped with a 785 nm laser source and a 0.85-m double monochromator. A spectroscopic ellipsometer (UVISEL-NIR, HORIBA Ltd.) was used to measure the refractive index at visible wavelengths. Semiconductor laser diodes operating at 1480 nm pumped the Er^{3+} ions, and the resulting fluorescence emissions were detected by a near-infrared photomultiplier tube (H10330-75, Hamamatsu) that was attached to a 1/4 m monochromator (Oriel MS257, Newport) equipped with a digital lock-in amplifier (Oriel Merlin™, Newport) A digital oscilloscope (HP 54501A, Hewlett-Packard) was also used to record the fluorescence decay profiles of the intra-4f-configurational transitions of Er^{3+} ions.

3. Results and discussion

3.1. Glass forming region and thermal properties

The glass forming region of the current SnO–MnO–P_2O_5 system was determined via visual-inspection followed by XRD and presented in Fig. 1. We obtained transparent glass phases when MnO content was less than 20 mol%. As for compositions including SnO of >45 mol%, most of the batches failed to melt. It is noteworthy that, in a SnO–P_2O_5 system, the incorporation of SnO of >65 mol% could form amorphous phases when melted in a N_2 atmosphere [9,15]. We believe that the reduced glass forming region confirmed in this study was caused mainly by the atmosphere during the melting process. However, under conventional processing conditions, it is likely that glass formation is limited by the content of MnO.

Characteristic temperatures along with the apparent densities of the PS and PM glasses are listed in Table 1. Most of the glasses showed T_g at below 350 °C, proving their potential as glass frit materials with a low softening temperature. The measured density marginally increased as SnO or MnO replaced P_2O_5, but the addition of SnO resulted in a larger change than MnO did. The molecular weight of each oxide was mostly responsible for the observation but its structural role in the glass network may have also contributed to variations in density. It is interesting to observe that T_g and T_x increased upon the addition of MnO, whereas such a tendency was not seen in the case of the SnO addition. As glass transition temperature is related to glass structures more closely than apparent density, the observed tendencies on thermal properties imply that MnO seems to influence a P_2O_5-based glass network more effectively than SnO. This is discussed below in more detail.

3.2. Compositional effects on the glass structures

Structural modifications induced by the addition of SnO and MnO on the glass network were studied in terms of Raman spectroscopy for both PS and PM glasses (Fig. 2). As summarized in Table 2, the characteristic vibration modes originating from phosphate polymeric structures were detected. As SnO and MnO replace P_2O_5, the peak centered at ~1150 cm^{-1} shifts to the lower energy side, and intensities of the peaks at ~300 cm^{-1}, ~520 cm^{-1}, ~700 cm^{-1} and ~920 cm^{-1} are reduced while the peak at ~1020 cm^{-1} seems to remain and slightly grow relative to other peaks at x = 45 mol%. Depending on the number of bridging oxygens within the phosphate tetrahedra [PO_4], phosphate glass exhibits characteristic Raman peaks at ~1150 cm^{-1}, ~1050 cm^{-1} and ~970 cm^{-1} for metaphosphate (PO_3^-, Q^2), pyrophosphate ($PO_{3.5}^{2-}$, Q^1) and orthophosphate (PO_4^{3-}, Q^0), respectively [9,26].

Table 1
Glass transition temperature (T_g), crystallization temperature (T_x) and density (d) of $(85-x)P_2O_5$–xSnO–15MnO (PS glasses, x = 30, 35, 40, 45) and $(55-y)P_2O_5$–45SnO–yMnO (PM glasses, y = 0, 5, 10, 15).

PS glass				PM glass			
x (mol%)	T_g (°C)	T_x (°C)	d (g/cm^3)	y (mol%)	T_g (°C)	T_x (°C)	d (g/cm^3)
30	320	421	3.27	0	266	354	3.39
35	311	441	3.24	5	288	–[a]	3.41
40	319	437	3.35	10	311	451	3.28
45	332	481	3.49	15	332	481	3.49

[a] Crystallization temperature was not clearly identified.

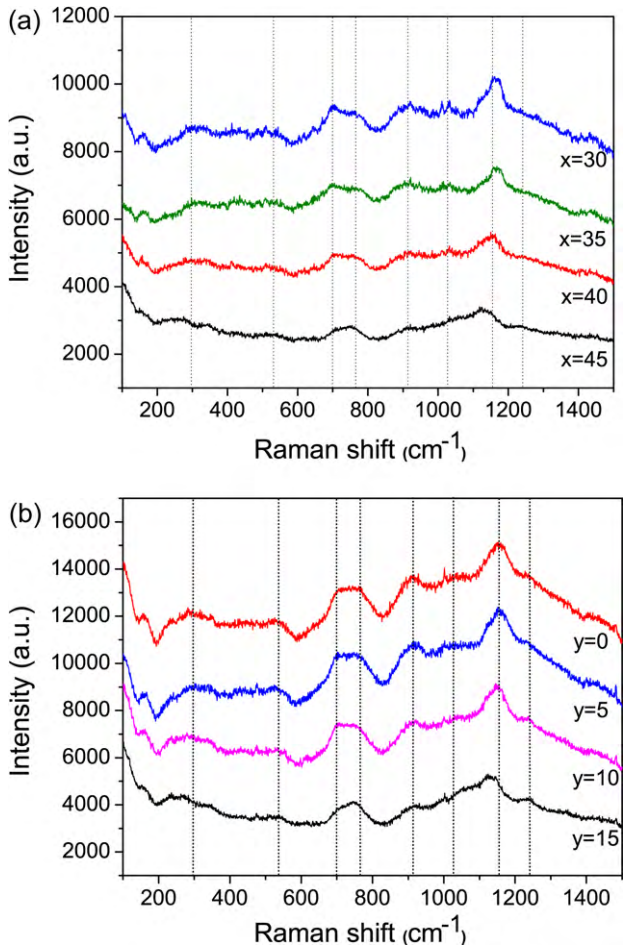

Fig. 2. Raman scattering spectra of (a) $(85-x)P_2O_5$–xSnO–15MnO (PS glasses x = 30, 35, 40, 45) and (b) $(55-y)P_2O_5$–45SnO–yMnO (PM glasses, y = 0, 5, 10, 15) (in mol%).

Although the variation is not so much significant, the shift of the ~1150 cm^{-1} peak to the lower energy side, together with the decrease of the P–O–P chain, indicates that SnO or MnO improves the pyrophosphate units within the network at the expense of the metaphosphate chains. Here, on this change of the phosphate network, no particular difference between SnO and MnO were identified from the Raman spectra, thus implying their similar structural roles. It is known that Sn resides in general as an Sn^{2+} state, and that the Sn–O–P bonds replace the P–O–P bonds in a SnO–P_2O_5 binary system [8,29]. Zotov et al. [22] also reported that Mn can be in its 2+, 3+ or 4+ state, resulting in a coordination number of 5.7 ± 0.4 within the metaphosphate glass, which indicates mixed coordination states between 4 and 6. Based on these previous results and the current Raman observations, it seems plausible that the structural roles of SnO and MnO are similar with each other, modifying the phosphate network and forming 4- or 6-coordinated local structures with the nearest neighboring oxygen ions supplied by the depolymerized phosphate network. The difference in the bonding strengths between the Mn–O–P and Sn–O–P units may thus support the change in T_g that is more clearly affected by the introduction of MnO, as can be seen in Table 1, and the less affected apparent density. Taking into consideration the possible presence of Sn^{4+} in the current glass system, the coordination number of Sn could differ from that of Mn. Although further detailed study is needed, this reasoning may explain the thermal behavior of the present glass system.

3.3. Optical properties

Fig. 3 shows the UV/VIS/NIR absorption spectra of PS and PM glasses. Both series of glasses turn out to be transparent above ~350 nm, suggesting their potential applicability in the visible wavelengths. As MnO gets incorporated into the glass, the absorption peak at around 410 nm grows, whereas the weak absorption tail near the Urbach edge emerges with the addition of SnO. The peak around 410 nm is attributed to the $^6A_1(S) \rightarrow {}^4T_2(G)$ transition of Mn^{2+} in tetrahedral sites [27]. Unlike the case of PbO–Nb_2O_5–P_2O_5 glass [27], absorptions due to Mn^{3+} and Mn^{2+} in octahedral sites, which appear near 490 nm and 520 nm, respectively, were not found from the present glasses. As such, these results indicate that Mn^{2+} ions mostly occupy the tetrahedral sites in the present glass system. The presence of localized states originating from the structural disorder, defects and impurities within the glass network is responsible for the weak absorption tail [30]. Although electronic absorption is normally dominant in the UV–VIS range, Rayleigh scattering induced by the density and concentrational fluctuation can also increase the background absorption and cannot be completely ruled out. Thus, it seems reasonable to assume their structural role which affects both optical and thermal properties as follows: SnO and MnO similarly depolymerize the phosphate chain network and MnO coordinates strongly with nearby oxygens while SnO simply improves the disorder or defects within the glass network. The optical bandgap (E_g^{opt}) was also estimated for the glasses using the relationship $h\nu\alpha \sim (h\nu - E_g^{opt})^2$ where α represents the absorption coefficient [31]. As shown in the inset figures of Fig. 3, the optical bandgap of the glasses was estimated to be 3.4–3.7 eV. The bandgap decreased with the addition of SnO, while a relatively small variation was detected for the MnO case.

Refractive index dispersion of PS and PM glasses is displayed in Fig. 4. Since the refractive index is closely related to the polarizability of constituents, the increase in the refractive index upon the introduction of transition metal ions, as shown in Fig. 4, seems to be reasonable. However, it is interesting that the refractive index increases with increasing MnO content up to 10 mol% and then decreases afterwards, whereas a monotonic increase of the refractive index is observed with increasing SnO content. Considering the multi-valency of Sn- and Mn-ion, the possible charge varia-

Table 2
Peak assignments of Raman spectra and their relevant literatures.

Peaks (cm^{-1})	Assignments	Ref.
~300	Bending vibrations related to O–P–O	[22,23]
~520	Network bending vibrations	[23]
~700	In-chain P–O–P symmetric stretching vibration	[24–26]
~750	Asymmetric vibrations of P–O–P chain in Q^2 species; Vibrations related to Mn–O group	[23,27]
~920	Vibration of $[PO_4]^{2-}$	[24,25,28]
~1020	Vibration of $[P_2O_7]^{4-}$ dimer or PO_2 symmetric stretching bands (Q^1)	[24,25,28]
~1150	Symmetric stretching vibration of PO_2 or O–P–O of corner sharing PO_4 (Q^2)	[24–26,28]
~1240	Symmetric and asymmetric stretching motions of NBO in Q^2	[23]

Q^i: Phosphate tetrahedral classification based on the number of bridging oxygen, i.

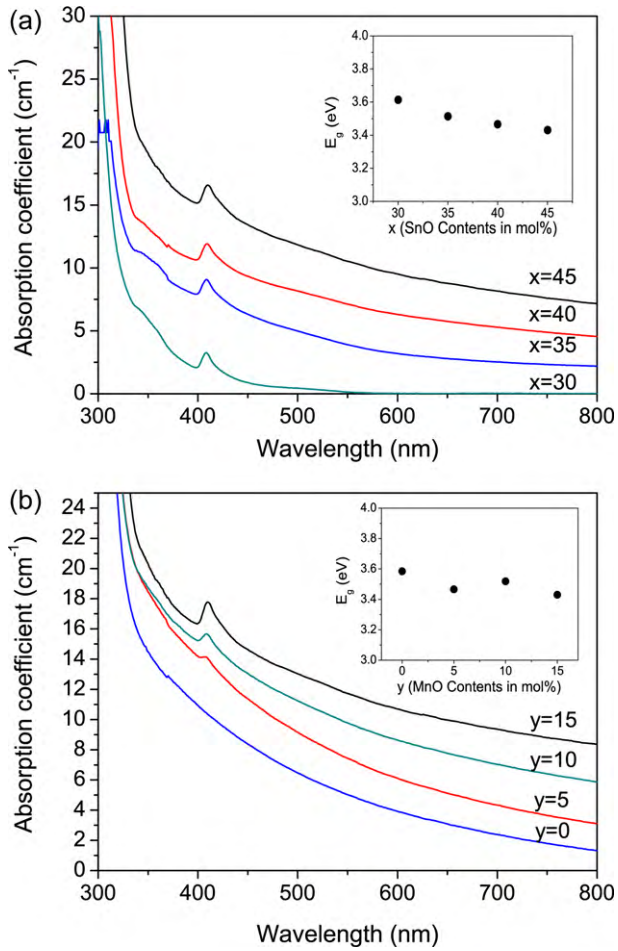

Fig. 3. Absorption spectra of (a) $(85-x)P_2O_5$–xSnO–15MnO (PS glasses x = 30, 35, 40, 45) and (b) $(55-y)P_2O_5$–45SnO–yMnO (PM glasses, y = 0, 5, 10, 15) (in mol%). Note that each spectrum was shifted in the y-axis scale for a clearer presentation. The inset figures show the variation of optical band gap with compositional change in each glass system.

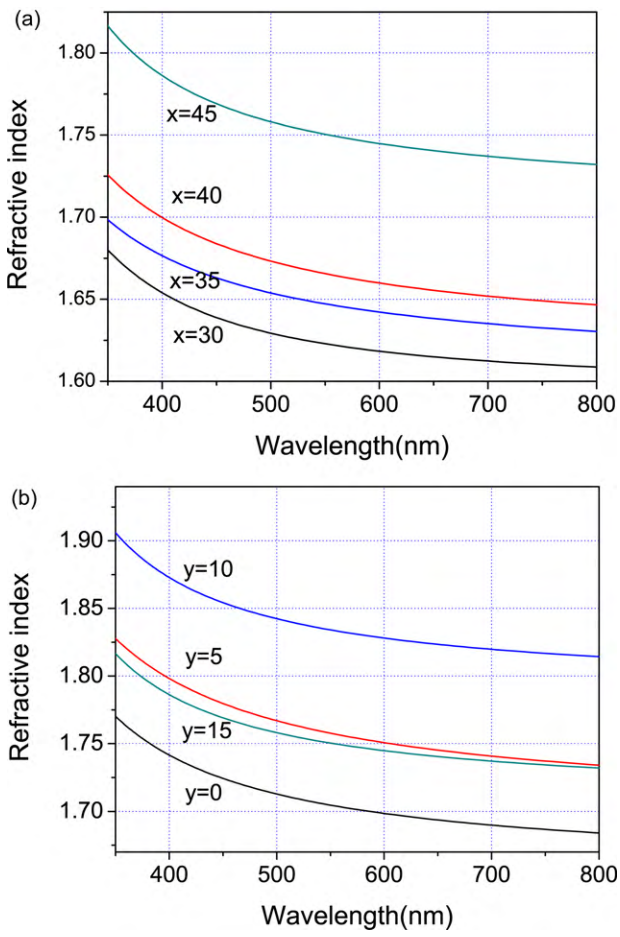

Fig. 4. Dispersion spectra of (a) $(85-x)P_2O_5$–xSnO–15MnO (PS glasses x = 30, 35, 40, 45) and (b) $(55-y)P_2O_5$–45SnO–yMnO (PM glasses, y = 0, 5, 10, 15) (in mol%).

tion of both ions after 10 mol% of MnO due to electronic interaction between the two ions would be responsible for the behavior; this needs further study in detail. Improved absorption of the probing light source in the visible range above 10 mol% of MnO may also affect the refractive index while measuring refractive index and cannot be completely ruled out.

3.4. Spectroscopic properties of Er^{3+}-ion

Absorption spectrum of Er^{3+} in P_2O_5–SnO–MnO glass system is shown in Fig. 5 which exhibits the characteristic absorption peaks due to the 4f–4f transition from the ground state ($^4I_{15/2}$) to the excited states. When pumped at 1480 nm, all glasses exhibited clear and strong emissions due to a $^4I_{13/2} \rightarrow {}^4I_{15/2}$ transition of trivalent Er-ions, as shown in Fig. 6. The effects of the compositional modifications on the spectral lineshape of this transition were examined by normalizing the emission spectra. As SnO and MnO were incorporated into the glass, a marginal decrease in the full width at half maximum (FWHM) was observed. The spectral lineshapes turned out to be nearly identical in the PS glass hosts, but a conspicuous change appeared in the PM glass hosts. Inhomogeneous broadening due to site-to-site variation in the local structures of rare-earth ions is mostly responsible for the FWHM, assuming similar transition behavior at each site [32]. As already mentioned above, the addition of SnO and MnO destroys the phosphate chains, and this structural adjustment is likely to result in more evenly distributed Er polyhedra in glasses [33]. Unlike the small variation in FWHM, the high- and low-energy sides of the $^4I_{13/2} \rightarrow {}^4I_{15/2}$ transition at around 1506 nm and 1605 nm, respectively, diminish as MnO modifies the glass structure with respect to the center peak at 1540 nm. Interaction between thermally populated Stark levels within the excited $^4I_{13/2}$ states along with the reduced inter-ionic distance between Er^{3+} ions in glasses promotes the evolution of those peaks [34]. Thus, it is plausible to assume that the inter-ionic distance between Er^{3+} ions extends upon the introduction of MnO, then

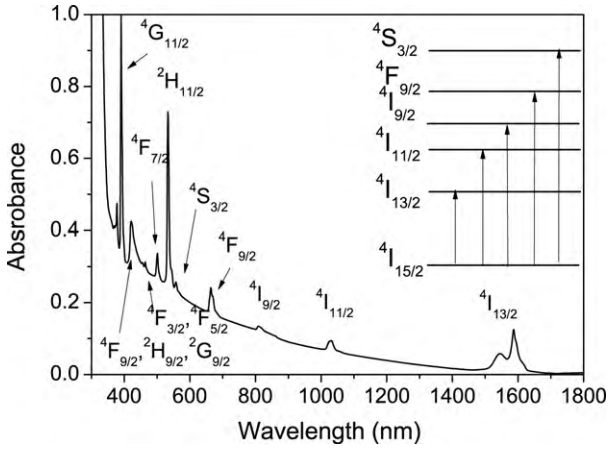

Fig. 5. UV/VIS/NIR absorption spectrum of Er^{3+}-doped $45P_2O_5$–45SnO–10MnO glass showing characteristic absorption transitions from the ground state ($^4I_{15/2}$).

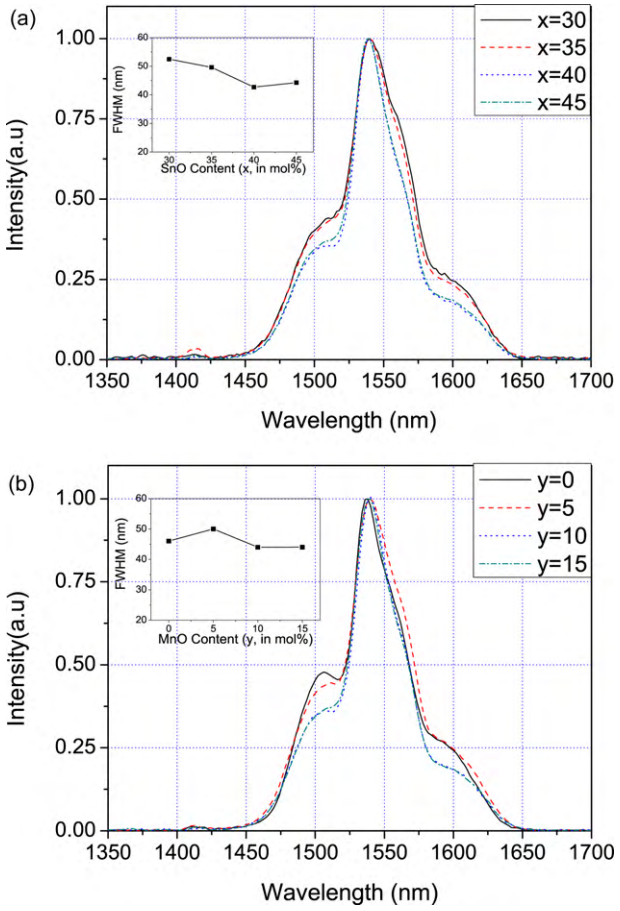

Fig. 6. Emission spectra of the Er^{3+}:$^4I_{13/2} \rightarrow {}^4I_{15/2}$ transition varying SnO and MnO content in (a) $(85-x)P_2O_5$–xSnO–15MnO (PS glasses x = 30, 35, 40, 45) and (b) $(55-y)P_2O_5$–45SnO–yMnO (PM glasses, y = 0, 5, 10, 15) (in mol%), respectively. The intensity was normalized to the maximum intensity for comparison. The inset figures show the change of full width at half maximum with SnO and MnO variation, respectively.

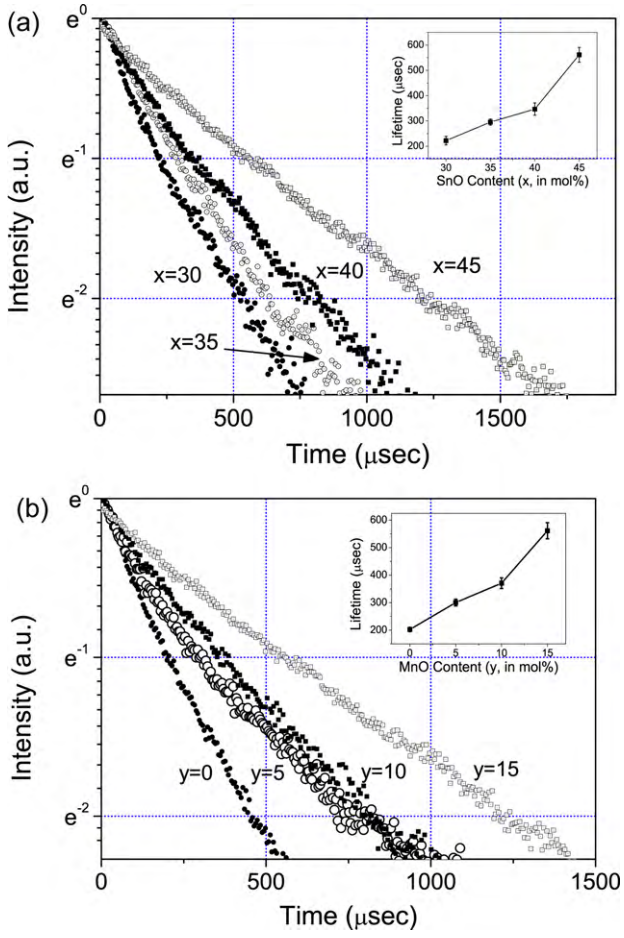

Fig. 7. Fluorescence decay curve of the Er^{4+}:$^4I_{13/2}$ state varying content of SnO and MnO in (a) $(85-x)P_2O_5$–xSnO–15MnO (PS glasses x = 30, 35, 40, 45) and (b) $(55-y)P_2O_5$–45SnO–yMnO (PM glasses, y = 0, 5, 10, 15) (in mol%), respectively. Inset figures show the estimated lifetime change with SnO and MnO variation, respectively.

reducing the interaction between the excited states and the side band transitions.

The lifetime of the excited state was determined from its first e-folding time for PS and PM glasses as depicted in Fig. 7. Almost pure exponential decay was observed for both glass systems, and the lifetime increased as the concentration of SnO and MnO increased. As the radiative lifetime is strongly dependent on the local phonon energy when the energy gap to the next lower-lying state is fixed [35], the enhancement can be mostly attributed to the modification of the local structure surrounding the Er^{3+}-ion. The shift of the main vibration mode at $\sim$1150 cm^{-1} to the low-energy side and the breaking of strong P_2O_5 network vibration modes as observed in Fig. 2 can also contribute to local phonon energy lowering. However, a relatively small shift of the vibration mode cannot by itself explain the lifetime improvement up to 3 times. Thus it seems more plausible that SnO and MnO modified the local structure neighboring the Er-ion into the lower phonon energy or further distributed Er-ion suppressing non-radiative energy transfer between Er-ions. The preferred location of the Er^{3+} ion nearby Sn–O or Mn–O coordinated polyhedra is mostly responsible for those behaviors practically influencing the enhanced lifetime but this needs further detailed study.

More detailed change of the local structure can be interpreted via Judd–Ofelt (J–O) analysis [36,37] which was performed for both glass systems based on the measured data and the following relationships.

$$P(aJ;bJ') = \frac{8\pi^2 m\nu_{ab}}{3hg_a}(\chi_{ed}S_{ed} + \chi_{md}S_{md}) \quad (1)$$

$$S_{ed}(aJ;bJ') = e^2 \sum_{t=2,4,6} \Omega_t \left|\left\langle 4f^N[\alpha,S,L]J \left\| U^{(t)} \right\| 4f^N[\alpha',S',L']J' \right\rangle\right|^2 \quad (2)$$

Here, $P(aJ;bJ')$ is the oscillator strength of the 4f–4f transition between $|aJ\rangle$ and $|bJ'\rangle$ manifolds [38] and S_{ed} and S_{md} are the line strengths due to electric and magnetic dipole–dipole transitions, respectively. χ_{ed} and χ_{md} are the local field correction factors for the electric dipole and the magnetic dipole transition, respectively. m, h and g_a represent the mass of the electron, the Planck constant and the degeneracy of $|aJ\rangle$ manifolds, respectively, while ν_{ab} and e are the mean frequency of the transition and the electric charge, respectively. $U^{2,4,6}$ stand for the reduced matrix elements of the transition and $\Omega_{2,4,6}$ are the J–O parameters which characterize the local environments surrounding the rare-earth ion [39,40]. S_{ed} mostly reflects the compositional effect as S_{md} is normally insensitive to the external parameters of a host matrix [41]. However, both line strengths were counted for the calculation of Judd–Ofelt parameters. The obtained J–O parameters obtained from the least squares fits to the measured oscillator strengths are summarized in Table 3 for both PS and PM glasses. Root-mean square (rms) deviation of the calculated oscillator strengths to evaluate quality of the fittings is also included, proving the goodness of the fitting com-

Table 3
The obtained Judd–Ofelt parameters and root-mean square deviation (δ_{rms}) for PS and PM glasses. Units of $\Omega_{2,4,6}$ are 10^{-20} cm^2 and RMS are 10^{-6}.

PS glass					PM glass				
x (mol%)	Ω_2	Ω_4	Ω_6	δ_{rms}	y (mol%)	Ω_2	Ω_4	Ω_6	δ_{rms}
30	0.76	0.42	0.84	0.068	0	3.96	1.09	0.54	0.055
35	0.10	0.54	0.74	0.058	5	4.79	0.70	0.22	0.032
40	3.15	0.79	0.57	0.019	10	4.30	0.80	0.22	0.041
45	3.57	0.95	0.38	0.038	15	3.57	0.95	0.38	0.038

pared to previous reports [16–20]. It is known that the covalence of chemical bonds between rare-earth and oxygen and the asymmetry or polarization of the local structure are closely related to the Ω_2 parameter [39,40,42,43].

As found in Table 3, Ω_2 increases as SnO content increases while it decreases after reaching maximum at 5 mol% with the addition of MnO. The result clearly indicates the sensitivity of the local structure of the Er^{3+} ion on SnO and MnO. The sensitivity further supports indirectly the preferred location of the Er-ion nearby a Sn–O or Mn–O coordinated structure which improved the measured lifetime. As discussed earlier, SnO and MnO both destroy the phosphate backbone but show different coordination within the glass network. Similarly, different contributions of SnO and MnO on the local structure of Er^{3+} were also observed. The covalence characteristic or the asymmetry of the Er–O polyhedra seems to evolve as SnO replaces P_2O_5 while it marginally reduces with MnO after the initial increase based on the Ω_2 parameter. Disordered structure with SnO and the preferred tetrahedral coordination of MnO could promote the change of Er–O coordination. Further study is required for the complete study of the local structure change with high resolution probing tool such as the extended X-ray absorption fine structure (EXAFS).

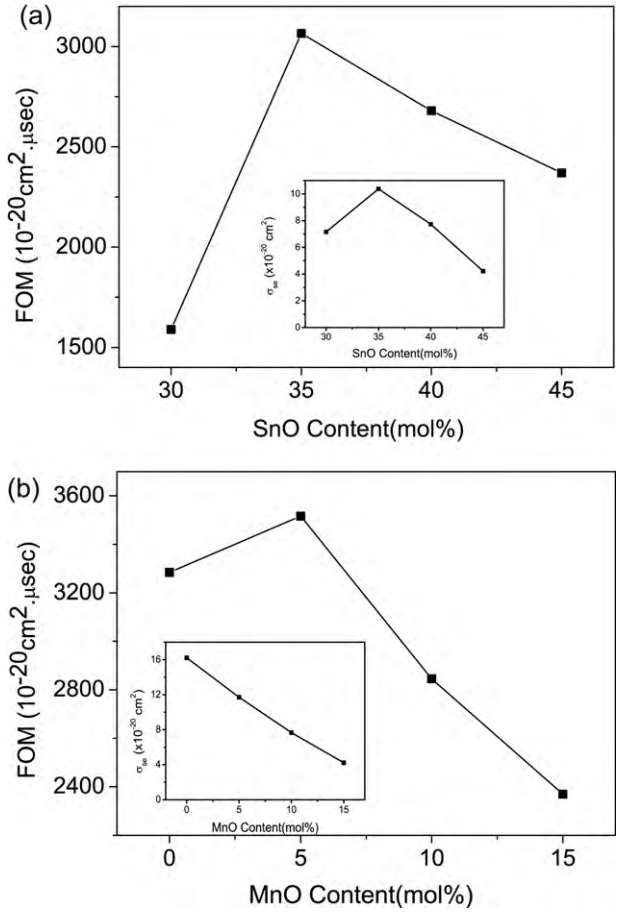

Fig. 8. The estimated FOM (figure of merit) values of Er^{3+} ions plotted as a function of (a) SnO and (b) MnO concentration in each glass system (in mol%). The inset figures represent the stimulated emission cross-section (σ_{se}) of Er^{3+}:$^4I_{13/2} \rightarrow {}^4I_{15/2}$ transition upon compositional change.

The stimulated emission cross-section (σ_{se}) of the Er^{3+}: $^4I_{13/2} \rightarrow {}^4I_{15/2}$ transition was estimated by using the Fütchtbauer–Ladenburg equation and the effective bandwidth of the emission transition, $\Delta\lambda_{eff}$.[45] The calculated value of σ_{se} plotted as a function of SnO or MnO content is shown in the inset of Fig. 8, which is quite comparable to that of other conventional laser materials [44,45]. This proves that the present ternary system is promising as a gain medium. The σ_{se} reaches the maximum at a SnO content of 35 mol%, and nominally decreases as MnO is added. The variations in the radiative transition probability, refractive index and $\Delta\lambda_{eff}$ may be responsible for these phenomena. Taking a closer look at the dependence of σ_{se} on the varying compositions, one can determine an optimum composition for optoelectronic applications. In an effort to find a practically feasible composition, figure of merits (FOMs) defined by the product of the stimulated emission cross-section and measured lifetime ($\sigma_{se}\cdot\tau_m$) were calculated for each glass. As exhibited in Fig. 8, the SnO and MnO contents of 35 mol% and 5 mol%, respectively, could be recommended for practical applications including amplifier or laser actions.

4. Conclusion

The glass forming region of the ternary phosphate system, SnO–MnO–P_2O_5 was verified and turned out to depend in a sensitive manner on MnO content. The glass transition temperature of the ternary glasses was quite low as 350 °C. SnO and MnO are likely to behave similarly in the glasses, i.e., they depolymerize the phosphate chains. No particular change in thermal properties and the increase in the tail absorption implied that SnO weakly coordinates and generates disorder or defects within the glass network. As MnO replaced the P_2O_5, however, T_g and the absorption band due to Mn^{2+} increased indicating the possible network strengthening due to the preferred tetrahedral coordination of the Mn-ion. The optical bandgap of 3.4–3.7 eV proved the high transparency and potential for optoelectronic applications which was also supported by the characteristic emission out of an Er^{3+}-ion. The variation of SnO and MnO content also affected the spectral properties of Er^{3+}-ions. Modification of the local structure nearby the Er^{3+}-ion was attributed to the spectroscopic difference between SnO and MnO varying samples. Based on Judd–Ofelt analysis, SnO is believed to improve the covalence behavior of Er–O bonds while MnO deteriorates it. Stimulated emission cross-sections and the figure of merits for the glasses also showed compositional dependency and proved their high potential as a gain medium.

Acknowledgment

This work was supported by the Korea Research Foundation Grant funded by the Korean Government (MOEHRD, Basic Research Promotion Fund) (KRF-2007-331-D00202).

References

[1] P. Subbalakshmi, N. Veeraiah, J. Phys. Chem. Solids 64 (2003) 1027.
[2] L. Bih, N. Allali, A. Yacoubi, A. Nadiri, D. Boudlich, M. Haddad, A. Levasseur, J. Phys. Chem. Glasses 40 (1999) 229.
[3] R.K. Brow, D.R. Tallant, J. Non-Cryst. Solids 222 (1997) 396.
[4] S.W. Lee, J.H. Lee, J. Phys. Chem. Glasses 36 (1995) 127.
[5] W. Matz, D. Stachel, E.A. Goremychkin, J. Non-Cryst. Solids 101 (1988) 80.
[6] R. Morena, J. Non-Cryst. Solids 263–264 (2000) 382.
[7] K. Morinaga, S. Fujino, J. Non-Cryst. Solids 282 (2001) 118.
[8] J. Cha, T. Kubo, H. Takebe, M. Kuwabara, J. Ceram. Soc. Japan 116 (2008) 915.
[9] A. Hayashi, T. Konishi, K. Tadanaga, T. Minami, M. Tatsumisago, J. Non-Cryst. Solids 345–346 (2004) 478.
[10] A.E. Marino, C.R. Arrasmith, L.L. Gregg, S.D. Jacobs, G. Chen, Y. Duc, J. Non-Cryst. Solids 289 (2001) 37.
[11] E.T.Y. Lee, E.R.M. Taylor, Opt. Mater. 28 (2006) 200.
[12] M. Sayer, A. Mansingh, Phys. Rev. B 6 (1972) 4629.
[13] B. Dutta, N.A. Fahmy, I.L. Pegg, J. Non-Cryst. Solids 251 (2005) 2552.
[14] M.M. El-Desoky, I. Kashif, Phys. Status Solidi (a) 194 (2002) 89.
[15] H. Takebe, W. Nonaka, T. Kubo, J. Cha, M. Kuwabara, J. Phys. Chem. Solids 68 (2007) 983.
[16] X. Yu, F. Song, W. Wang, L. Luo, L. Han, Z. Cheng, T. Sun, J. Tian, E.Y.B. Pun, J. Appl. Phys. 104 (2008) 113105.
[17] Y. Fang, L. Hu, L. Wen, M. Liao, J. Alloys Compd. 431 (2007) 246.
[18] J.A. Valles, M.A. Rebolledo, J. Used, Opt. Mater. 31 (2009) 1346.
[19] A. Florez, E.M. Ulloa, R. Cabanzo, J. Alloys Compd. 488 (2009) 606.
[20] K. Pradeesh, C.J. Oton, V.K. Agotiya, M. Raghavendra, G. Vijaya Prakash, Opt. Mater. 31 (2008) 155.
[21] B.-C. Hwang, S. Jiang, T. Luo, K. Seneschal, G. Sorbello, M. Morrell, F. Smektala, S. Honkanen, J. Lucas, N. Peyghambarian, IEEE Photon. Technol. Lett. 13 (2001) 197.
[22] N. Zotov, H. Schlenz, B. Brendenbach, H. Modrow, J. Hormes, F. Reinauer, R. Glaum, A. Kirfel, C. Paulmann, N. Naturforsch. 58a (2003) 419.
[23] M.A. Karakassides, A. Saranti, I. Kouteselas, J. Non-Cryst. Solids 347 (2004) 69.
[24] N. Vedeanu, O. Cozar, I. Ardelean, B. Lendl, D.A. Magdas, Vibr. Spectrosc. 48 (2008) 259.
[25] D. Boudlich, L. Bih, M.E. Hassane Archidi, M. Haddad, A. Yacoubi, A. Nadiri, B. Elouadi, J. Am. Ceram. Soc. 85 (2002) 632.
[26] R.K. Brow, J. Non-Cryst. Solids 263–264 (2000) 1.
[27] N. Krishna Mohan, M. Rami Reddy, C.K. Jayasankar, N. Veeraiah, J. Alloys Compd. 458 (2008) 66.
[28] I. Ardelean, D. Rusu, C. Andronache, V. Ciobota, Mater. Lett. 61 (2007) 3301.
[29] C.M. Shaw, J.E. Shelby, J. Am. Ceram. Soc. 71 (1988) C252.
[30] D.L. Wood, J. Tauc, Phys. Rev. B 5 (1972) 3144.
[31] S.R. Elliott, Physics of Amorphous Materials, Longman Scientific & Technical, Harlow, U.K., 1990, pp. 340–380.
[32] W.M. Yen, P.M. Selzer, Laser Spectroscopy of Solids, Springer-Berlang, Berlin, 1986.
[33] W.J. Chung, Y.G. Choi, J. Am. Ceram. Soc. 93 (2010) 1432.
[34] W.J. Chung, A. Jha, S. Shen, P. Joshi, Phil. Mag. 84 (2004) 1197.
[35] C.B. Layne, W.H. Lowdermilk, M.J. Weber, Phys. Rev. B 16 (1977) 10.
[36] B.R. Judd, Phys. Rev. 127 (1962) 750.
[37] G.S. Ofelt, J. Chem. Phys. 37 (1962) 511.
[38] R. Reisfeld, C.K. Jorgensen, Lasers and Excited States of Rare Earths, Springer-Verlag, Berlin, 1977, pp.64-122.
[39] S. Tanabe, T. Ohyagi, N. Soga, T. Hanada, Phys. Rev. B 46 (1992) 3305.
[40] H. Li, S.K. Sundaram, P.A. Blanc-Pattison, L. Li, J. Am. Ceram. Soc. 85 (2002) 1377.
[41] C. Görller-Walrand, K. Binnemans, in: K.A. Gschneidner Jr., L. Eyring (Eds.), Handbook on the Physics and Chemistry of Rare Earths, vol. 25, Elsevier Science Publishers B. V., Amsterdam, Netherlands, 1998.
[42] M.B. Saisudha, J. Ramakrishna, Phys. Rev. B 53 (1996) 6186.
[43] Y.G. Choi, J.H. Song, Y.B. Shin, J. Heo, J. Non-Cryst. Solids 353 (2007) 1665.
[44] M.J. Weber, D.C. Ziegler, C.A. Angell, J. Appl. Phys. 53 (1982) 4344.
[45] G.A. Kumar, R. Riman, S.C. Chae, Y.N. Jang, I.K. Bae, H.S. Moon, J. Appl. Phys. 95 (2004) 3243.